International Journal of Numerical Methods for Heat & Fluid Flow

2813

Received 29 November 2024
Revised 4 January 2025
Accepted 12 January 2025

Membrane-driven flow and heat transfer of viscoelastic fluids: MHD and entropy generation analysis

Abhishesh Pandey
Department of Mathematics and Statistics, Manipal University Jaipur, Jaipur, India

Ashvani Kumar and Dharmendra Tripathi
Department of Mathematics, National Institute of Technology Uttarakhand, Srinagar (Garhwal), India, and

Kalpna Sharma
Department of Mathematics and Statistics, Manipal University Jaipur, Jaipur, India

Abstract

Purpose – The complex behavior of viscoelastic fluids and its flow analysis under the impact of transverse magnetic field are becoming increasingly important in numerous emerging applications including biomedical engineering, aerospace engineering, geophysics and industrial applications. Additionally, the thermal analysis and fluid flow driven by propagating membranes will aid significant applications for microscale transport in bio-thermal systems. This study aims to investigate the thermal effects of viscoelastic fluids driven by membrane-induced propagation and transverse magnetic field.

Design/methodology/approach – The propagation of the membranes will work as pump which pushes the fluids from bottom to top against the gravitation force; however, there is backflow due to compression and expansion phases of membrane propagation. The Jeffrey fluid model is employed to analyze the viscoelastic fluid flow, with entropy generation examined and equations solved analytically under low Reynolds number and long-wavelength assumptions.

Findings – The findings reveal that an increase in magnetic field strength impedes fluid flow, while higher values of the Grashof number, heat source parameter and Jeffrey fluid parameter enhance fluid motion. The study's findings have significant implications for optimizing magnetohydrodynamic systems in various emerging applications, including biomedical engineering, aerospace, geophysics and industrial processes.

Originality/value – This study aims to investigate the impact of a transverse magnetic field on the flow and heat transfer characteristics of viscoelastic fluids driven by membrane propagation.

Keywords Propagating membrane, Heat transfer, Viscoelastic fluid, Entropy generation, Magnetohydrodynamics, Biothermal system

Paper type Research paper

1. Introduction

In the fluid dynamics, exploring the non-Newtonian fluid is crucial phenomena due to their unique and intricate functioning in various industrial and engineering applications. In

© Abhishesh Pandey, Ashvani Kumar, Dharmendra Tripathi and Kalpna Sharma. Published by Emerald Publishing Limited. This article is published under the Creative Commons Attribution (CC BY 4.0) licence. Anyone may reproduce, distribute, translate and create derivative works of this article (for both commercial and non-commercial purposes), subject to full attribution to the original publication and authors. The full terms of this licence may be seen at http://creativecommons.org/licences/by/4.0/legalcode

International Journal of Numerical Methods for Heat & Fluid Flow
Vol. 35 No. 8, 2025
pp. 2813-2840
Emerald Publishing Limited
0961-5539
DOI 10.1108/HFF-11-2024-0898

Downloaded from http://ftp.nowpublishers.com/hff/article-pdf/35/8/2813/10338472/hff-11-2024-0898en.pdf by guest on 01 June 2026

contrast to Newtonian fluids like water and air, which exhibit constant viscosity regardless of shear rate, non-Newtonian fluids have viscosities that vary with shear strain rate. This phenomenon is crucial in understanding the mechanism of incompressible, stretchy fluid behavior when the waves traveling along the tube's wall (Böhme and Friedrich, 1983). Lindner *et al.* (2002) examined fluid movement in narrow spaces with both rigid and flexible polymers, noting that flexible polymers create varying pressure while maintaining the same flow. Hosseini *et al.* (2007) introduced a smooth particle hydrodynamic method for non-Newtonian fluid flow, adopting Lagrangian approach and unique viscous term treatment inspired by the Eulerian methods. Based on LBM (Lattice Boltzmann Method), Yoshino *et al.* (2007) applied this to simulate incompressible non-Newtonian fluids, including shear thickening and shear thinning types. Esmael *et al.* (2010) studied the flow of shear-thinning fluids in pipe and highlighted how shear-thinning properties affects the flow characteristics in the confined geometries. By using Adomian decomposition method, Tripathi (2011) analyzed that how relaxation time, fractional parameter and wave amplitude influence the flow. These studies provide insights into the distinctive flow properties of shear-thinning and viscoelastic non-Newtonian fluids, enhancing our understanding of their behavior for varying flow conditions and constraints.

In the continuation of the non-Newtonian fluid, viscoelastic fluid (Jeffrey fluid model) is characterized by both viscous and elastic properties. Jeffrey fluids demonstrate stress relaxation, allowing them to flow like a liquid while also possessing elastic properties that enable them to return to their initial shape. Hayat *et al.* (2007) studied the peristaltic motion of the Jeffrey fluid in a circular tube and found that the net flow rate's oscillatory behavior in the Jeffrey fluid is lower in the comparison of the Maxwell fluid. Nadeem and Akbar (2009) examined how variable viscosity influences the flow of incompressible Jeffrey fluids within an asymmetric channel, applying Reynolds viscosity model. Pandey and Tripathi (2010) studied the transport of a viscoelastic fluid through peristaltic motion in a channel and a circular tube, employing the Jeffrey fluid model. Akbar *et al.* (2011) examined the blood flow in a narrowed, tapered artery where the blockage or stenosis is present. This Jeffrey fluid model helps to capture the complex behavior, accounting for both its viscous and elastic characteristic, which varies with the flow conditions. Ellahi *et al.* (2014) have explored a mathematical model that describes how Jeffrey fluid moves through narrow tapered arteries affected by the atherosclerosis, which provides better understanding of blood flow in arteries with plaque buildup and may improve our understanding of cardiovascular diseases and potential treatments. Liao (2003) applied the Homotopy analysis method to demonstrate that magnetic fields enhance skin friction in shear-thinning fluids flowing over a stretching sheet. Tripathi and Bég (2012) examined the peristaltic flow of couple stress fluid within gap between two coaxial channels which include an annular porous channel influenced by the presence of magnetic field.

Heat transfer is the process by which the thermal energy transferred from one body or substance to another, which occurs primarily three mechanisms i.e., conduction, convection and radiation. Bhatti *et al.* (2024) analyzed third-grade fluid motion through vertical walls with nanofluid infusion, examining effects of magnetic/electric fields, viscosity, temperature rise and joint lubrication. Yadeta and Shaw (2023) investigated blood flow and magnetic nanoparticle transport in a stenosed artery, demonstrating the significance of parameter effects for drug delivery and cardiovascular therapies. Shaw *et al.* (2023) analyzed magnetic drug targeting in Jeffrey fluid, revealing enhanced drug delivery efficiency influenced by memory effects, magnetization and nanoparticle volume fraction. Bhatti *et al.* (2016) explored effects of variable magnetic fields on peristaltic Jeffrey fluid flow in nonuniform rectangular ducts with compliant walls. Kumar *et al.* (2024) examined the impact of the viscoelastic fluid and surface roughness in the diverging channel for physiological fluid.

Downloaded from http://ftp.nowpublishers.com/hff/article-pdf/35/8/2813/10338472/hff-11-2024-0898en.pdf by guest on 01 June 2026

Metzner (1965) reviewed recent research on heat transfer in non-Newtonian fluids, providing a summary of earlier studies. Tsai *et al.* (2008) investigated the effects of a spatially varying heat source or sink on flow dynamics and heat transfer over an unsteady stretching sheet in a stationary fluid. Prommas (2011) conducted experimental validation of a combined mass and thermal model for convective drying in multi-layered packed beds composed of glass beads, water and air. Shojaeian and Koşar (2014) analyzed that how efficiently heat transfer through different types of fluids with different boundary conditions. Magesh and Kothandapani (2021) considered the Johnson-Segalman fluid in an asymmetrically curved channel and studied peristaltic flow by incorporating heat and mass transfer. Yusuf *et al.* (2024) explored the use of graphene oxide nanoparticles in vacuum residue fluid for enhanced oil recovery, utilizing computational models to optimize efficiency. Aslam *et al.* (2024) developed a hybrid firefly-water cycle algorithm to optimize nonlinear Hall currents and electric double layer effects in multiphase wavy flow, enhancing accuracy and efficiency. Vajravelu *et al.* (2011) investigated heat transfer in Jeffrey fluid flow within a vertical porous layer, considering long-wavelength approximations and low Reynolds number conditions. Turkyilmazoglu and Pop (2013) explored how Jeffrey fluid flow and transfer of heat near a stagnation point on a sheet that is either stretching or shrinking, with an external flow moving parallel to it. Ellahi and Hameed(2012) examined thermal properties in both Newtonian and non-Newtonian fluids including Jeffrey and third grade types fluids confined between parallel plate, incorporating velocity slip effects under isothermal and uniform heat flux boundary conditions. Ellahi (2013) investigated the influence of magnetohydrodynamics (MHD) and variable viscosities on the flow of non-Newtonian nanofluids in a pipe under constant pressure. Elelamy *et al.* (2020) presented a mathematical model and numerical simulation for bacterial growth in heart valves, incorporating non-Newtonian fluid flow, nanoparticles and magnetic fields. Kothandapani and Pushparaj (2017) analyzed the combined effects of induced magnetic fields and thermal radiation on Carreau nanofluid peristaltic transport in a tapered asymmetric channel, using analytical solutions. Bhatti *et al.* (2022) analyzed entropy generation and thermal behavior of magnetic hybrid nanofluid (Au-Ag/NPs) in Eyring-Powell fluid, examining its effects on velocity, temperature and pumping characteristics, with potential applications in pharmaceuticals. Ramadan *et al.* (2025) developed a poroelastic model to investigate temperature increases in knee cartilage under cyclic sinusoidal loading. Some studies incorporated the effect of Joule and Newtonian heating at Jeffrey fluid on stretching sheet influenced by magnetic field with heat source/sink (Idowu *et al.*, 2013**;** Farooq *et al.*, 2015). Hayat *et al.* (2015) focused on analyzing the momentum and thermal boundary layers in the flow of a viscoelastic Jeffrey fluid over an exponentially stretching sheet. Furthermore, Sen *et al.* (2021) examined the effects of Newtonian cooling, magnetic fields, and nonlinear radiation on Jeffrey fluid flow near a stagnation point, highlighting potential industrial applications in plastic and food processing. Membrane pumping mechanism can have significant impact to control fluid behavior in the various application in biomedical devices, microfluidic system and industrial cooling, where precise fluid control and efficient heat transfer are essential.

Membrane pumping mechanism is a microfluidic solution for enhanced fluid flow; where traditional pumping methods fall short, membrane-based pumps offer a viable alternative. By periodically expanding and contracting a flexible membrane, these pumps create fluid flow through microchannels, particularly in biological and microfluidic applications. Researchers and engineers have continually refined membrane pump design for optimized performance. Aboelkassem and Staples (2013) investigated a bioinspired model shows that rhythmic wall contractions in an inelastic tube with two constriction sites, which is generating unidirectional flow with low Reynolds number approximation. Cai *et al.* (2016)

Downloaded from http://ftp.nowpublishers.com/hff/article-pdf/35/8/2813/10338472/hff-11-2024-0898en.pdf by guest on 01 June 2026

described advanced valving pumping mechanism designed for an elastic polymer-based centrifugal microfluidic platform. Tripathi *et al.* (2023) reviewed on the discrete scheme membrane-based pumping mechanism, which highlights the potential of these mechanisms for advanced micro-flow systems in medical, bio-engineering and microfabrication applications. Furthermore, Bhandari *et al.* (2022b) and Bhandari and Tripathi (2022) analyzed the thermal behavior in a finite-length vertical microchannel. The pumping model evaluated the streamlines and isotherms for key parameters during the contraction and expansion phases of membrane motion. Bhandari *et al.* (2022a) analyzed transient viscous flow in a microchannel driven by propagating membrane pumping under the influence of electric and magnetic fields. Building on such membrane-driven flow models, Pandey *et al.* (2024) recently investigated the effects of viscoelastic fluid in a porous medium subjected to an electric field within an asymmetric microchannel.

After the comprehensive investigation of existing literature on magneto-viscoelastic flow and heat transfer, and propagating membrane driven flow, this research aims to explore a novel and unexplored model for heat transfer and magneto-viscoelastic flow driven by propagating membranes. A mathematical model is formulated to explore the unique phenomenon of magneto-viscoelastic flow induced by a membrane pumping mechanism. Moreover, entropy generation analysis for the present model is discussed. And the analytical solutions of governing equations for this model have been derived by using the assumptions of low Reynolds number. Present study examines the impact of various parameters like Grashof number, Hartmann number, Heat source parameter, Jeffrey fluid parameter, Brinkman number, relative temperature and membrane shape parameter on the variation in fluid flow characteristics including axial and transverse velocity profile, pressure gradient, pressure distribution, entropy generation, volumetric flow rate, variation in heat transfer, wall shear stress and streamline patterns. The results of this study are anticipated to improve the understanding of membrane-driven flow propagation in non-Newtonian fluids in magnetohydrodynamic framework. The membrane pumping mechanism's future scope includes miniaturization, material innovations and optimization algorithms for enhanced performance in microfluidic and biomedical applications.

2. Formulation of the problem

2.1 Problem definition

Present study examines heat transfer with magneto-viscoelastic flow driven by propagating membranes. The wall geometry is depicted in Figure 1, which shows a vertical microchannel with length L and width b, propagated by single membrane of length $2\bar{a}$. The membrane's propagation causes the fluid to move in both forward and backward directions. The wall deformation is considered periodic, resulting from the motion caused by membrane contraction. The phase of expansion and contraction in membrane motion can be mathematically expressed as follows (Bhandari *et al.*, 2022a):

$$\bar{h}(\bar{x},\bar{t}) = \begin{cases} \frac{b}{2},\psi & -\frac{L}{2} \le \bar{x} < -\bar{a} \\ \frac{b}{2} + 2\bar{a}_0 \left(\frac{\bar{x}}{\bar{a}}\right)^{2M} - 1 \Big)^3 h_{memb}(\bar{x},\bar{t}),\psi & -\bar{a} \le \bar{x} \le \bar{a} \\ \frac{b}{2},\psi & \bar{a} < \bar{x} \le \frac{L}{2} \end{cases}, \psi \tag{1}$$

Downloaded from http://ftp.nowpublishers.com/hff/article-pdf/35/8/2813/10338472/hff-11-2024-0898en.pdf by guest on 01 June 2026

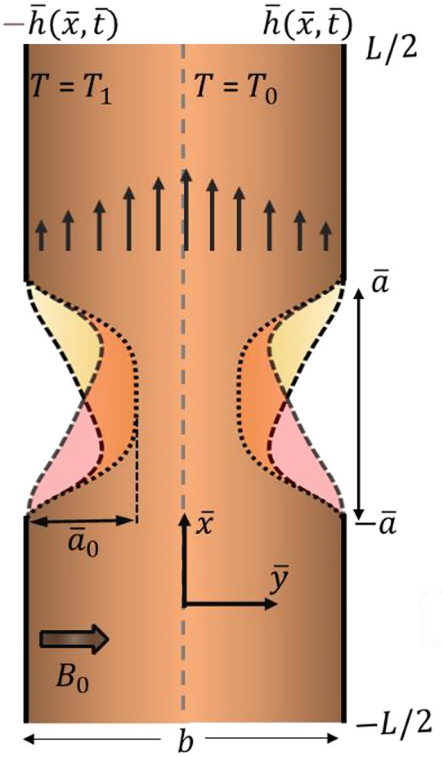

Source(s): Figure by authors

Figure 1. Schematic diagram of propagating membrane-driven viscoelastic fluids flow and heat transfer in presence of transverse magnetic field

where, $h_{memb}(\bar{x},\bar{t}) = (1-\bar{x}k_0\cos(\pi f\bar{t}))\sin^2(\pi f\bar{t})$ is the membrane kinematic profile, M is the membrane parameter which define its shape, $\bar{a}_0$ denotes the amplitude of membrane contraction, $\bar{a}$ specifies the membrane's axial length, k_0 characterizes the optical parameter defining the membrane shape and f denotes the frequency; this represents the rhythmic propagation of the membrane, contributing to the development of pressure within the microchannel.

2.2 Governing equations

In this study, an incompressible, two-dimensional, transient viscoelastic fluid flow under laminar conditions, driven by membrane contraction along a finite and vertical microchannel with an applied transverse magnetic field, has been examined. To analyze the heat transfer, energy equation is considered. The length of the microchannel is assumed to be large in comparison to the width of the microchannel $\left(\delta = \frac{b}{L} \ll 1\right)$. The governing equation for the additional stress $\bar{\tau}$ for the Jeffrey fluid is given as (Pandey and Tripathi, 2010):

$$\bar{\tau} = \frac{\mu}{1+\lambda_1}\{\dot{\gamma} + \lambda_2\ddot{\gamma}\}, \tag{2}$$

Downloaded from http://ftp.nowpublishers.com/hff/article-pdf/35/8/2813/10338472/hff-11-2024-0898en.pdf by guest on 01 June 2026

where $\dot{\gamma}$, μ, λ_1 and λ_2 are the rate of strain, viscosity, ratio of relaxation to retardation times, and dots denote the differentiation with respect to time. On simplification of equation (2), the stress term $\overline{\tau}_{\overline{x}\overline{y}}$ reduces to following form:

$$\overline{\tau}_{\overline{x}\overline{y}} = \frac{\mu}{1+\lambda_1}\left(1+\lambda_2\left[\overline{u}\frac{\partial}{\partial\overline{x}}+\overline{v}\frac{\partial}{\partial\overline{y}}\right]\right)\left(\frac{\partial\overline{v}}{\partial\overline{x}}+\frac{\partial\overline{u}}{\partial\overline{y}}\right). \tag{3}$$

The governing equations for mass, momentum and energy conservation are considered as (Tripathi and Bég, 2012; Vajravelu *et al.*, 2011):

$$\frac{\partial\overline{u}}{\partial\overline{x}}+\frac{\partial\overline{v}}{\partial\overline{y}}=0, \tag{4}$$

$$\rho\left(\frac{\partial}{\partial\overline{t}}+\overline{u}\frac{\partial}{\partial\overline{x}}+\overline{v}\frac{\partial}{\partial\overline{y}}\right)\overline{u}=-\frac{\partial\overline{p}}{\partial\overline{x}}+\frac{\partial\overline{\tau}_{\overline{x}\overline{x}}}{\partial\overline{x}}+\frac{\partial\overline{\tau}_{\overline{x}\overline{y}}}{\partial\overline{y}}-\sigma B_0^2\overline{u}+\rho g\alpha(\overline{T}-T_0), \tag{5}$$

$$\rho\left(\frac{\partial}{\partial\overline{t}}+\overline{u}\frac{\partial}{\partial\overline{x}}+\overline{v}\frac{\partial}{\partial\overline{y}}\right)\overline{v}=-\frac{\partial\overline{p}}{\partial\overline{y}}+\frac{\partial\overline{\tau}_{\overline{y}\overline{x}}}{\partial\overline{x}}+\frac{\partial\overline{\tau}_{\overline{y}\overline{y}}}{\partial\overline{y}}, \tag{6}$$

$$\rho C_p\left(\frac{\partial}{\partial\overline{t}}+\overline{u}\frac{\partial}{\partial\overline{x}}+\overline{v}\frac{\partial}{\partial\overline{y}}\right)T=k\left(\frac{\partial^2T}{\partial\overline{x}^2}+\frac{\partial^2T}{\partial\overline{y}^2}\right)+\varphi, \tag{7}$$

where, $\bar{u}$ and $\overline{v}$ represent the velocities in the $\overline{x}$ and $\overline{y}$ directions, respectively. The other parameters are defined as follows: ρ is the density, $\overline{t}$ is time, $\overline{p}$ is pressure, α is the coefficient of linear thermal expansion, φ is the heat source parameter, k is the thermal conductivity, T is temperature, C_p is the specific heat at constant pressure, B_0 is the magnetic field and $\overline{\tau}_{\overline{x}\overline{x}}$, $\overline{\tau}_{\overline{x}\overline{y}}$, $\overline{\tau}_{\overline{y}\overline{x}}$, $\overline{\tau}_{\overline{y}\overline{y}}$ are the components of the extra stress.

2.3 Dimensional analysis

The following nondimensional variables are incorporated as:

$$x=\frac{\overline{x}}{L},\ y=\frac{\overline{y}}{b},\ t=\frac{\overline{t}}{L/u_0},\ u=\frac{\overline{u}}{u_0},\ v=\frac{\overline{v}}{u_0\delta},\ p=\frac{\overline{p}b^2}{\mu L u_0},\ h=\frac{\overline{h}}{b},$$

$$\theta=\frac{T-T_0}{T_1-T_0},\ \beta=\frac{b^2\varphi}{k(T_1-T_0)},\ Ha=B_0b\sqrt{\frac{\sigma}{\mu}},\ Gr=\frac{\rho gb^2\alpha(\overline{T}_1-T_0)}{\mu u_0},\ Re=\frac{\rho bu_0}{\mu},\ \delta=\frac{b}{L},\ \tau=\frac{b\overline{\tau}}{\mu u_0}. \tag{8}$$

Here, u_0 denotes the reference velocity, δ represents the ratio of the width and length, θ is the non-dimensional form of temperature, β denotes heat source parameter. Additionally, *Gr* and *Re* are Grashof number and Reynolds number, respectively. The symbols used without bar are same meaning as without dimension. By taking the approximations i.e., $\delta \ll 1$ and $Re \ll 1$, the fundamental equations (4)–(7) are transformed as:

$$\frac{\partial u}{\partial x}+\frac{\partial v}{\partial y}=0, \tag{9}$$

Downloaded from http://ftp.nowpublishers.com/hff/article-pdf/35/8/2813/10338472/hff-11-2024-0898en.pdf by guest on 01 June 2026

$$\frac{\partial p}{\partial x} = \frac{1}{1+\lambda_1}\frac{\partial^2 u}{\partial y^2} - Ha^2 u + Gr\theta, \psi \tag{10}$$

$$\frac{\partial p}{\partial y} = 0, \psi \tag{11}$$

$$\frac{\partial^2 \theta}{\partial y^2} + \beta = 0. \psi \tag{12}$$

From equation (11), it can be observed that pressure remains unaffected by the variation in y, that means pressure is only function of x and time t. The equations (9)–(12) are simplified using the provided boundary conditions:

$$\frac{\partial \theta}{\partial y}|_{y=0} = 0,\ \theta|_{y=h} = 1,$$

$$\frac{\partial u}{\partial y}|_{y=0} = 0,\ u|_{y=h} = 0,\ v|_{y=0} = 0,\ v|_{y=h} = \frac{\partial h}{\partial t}. \psi \tag{13}$$

The above boundary conditions are considered based on the physical model which are defined as:

- a minimum temperature at the microchannel wall ($y = h$) while the maximum temperature at the center ($y = 0$) are considered;
- no-slip condition at the wall ($y = h$) and a regularity condition ($\partial u/\partial y = 0$) at the center ($y = 0$) are considered; and
- the transverse velocity at the center of the microchannel remains zero, indicating no fluid movement, while at the wall, it is determined by the rate of change of the microchannel's wall, reflecting dynamic boundary conditions due to the propagation of membranes fitted to the microchannel.

2.4 Analytical solutions

The temperature can be calculated by integrating equation (12) and using the boundary conditions defined in equation (13) as follows:

$$\theta = 1 + \frac{1}{2}\beta\ h^2 - y^2). \psi \tag{14}$$

The expression for the axial velocity can be determined by solving equation (10) with the boundary conditions defined in equation (13) as:

$$u = \frac{cosh\ \ y\ \ Ha\ \sqrt{1+\lambda_1})))}{cosh\ \ h\ \ Ha\ \sqrt{1+\lambda_1})))}\left(\frac{1}{Ha^2}\frac{\partial p}{\partial x} + \frac{Gr\beta}{Ha^4(1+\lambda_1)\leftarrow} - \frac{Gr}{Ha^2}\right.$$
$$\left. - \frac{1}{Ha^2}\frac{\partial p}{\partial x} + \frac{1}{2}\ \ \frac{Gr\beta\ h^2}{Ha^2}\right(-y^2)\left(-\frac{Gr\beta}{Ha^4(1+\lambda_1)\leftarrow} + \frac{Gr}{Ha^2}. \psi \right. \tag{15}$$

Downloaded from http://ftp.nowpublishers.com/hff/article-pdf/35/8/2813/10338472/hff-11-2024-0898en.pdf by guest on 01 June 2026

The solution of transverse velocity can be obtained from equation (9) and equation (15) with the boundary conditions defined in equation (13) as:

$$v = \operatorname{sech}\left(h\,Ha\,\sqrt{1+\lambda_1}\right)\left(\tanh\left(h\,Ha\,\sqrt{1+\lambda_1}\right)\sinh\left(y\,Ha\,\sqrt{1+\lambda_1}\right)\left(\frac{1}{Ha^2}\frac{\partial p}{\partial x} + \frac{Gr\beta}{Ha^4(1+\lambda_1)} - \frac{Gr}{Ha^2}\frac{\partial h}{\partial x}\right) - \frac{1}{Ha^2}\frac{\partial^2 p}{\partial x^2}\left(\frac{\sinh\left(y\,Ha\,\sqrt{1+\lambda_1}\right)}{Ha\,\sqrt{1+\lambda_1}} - \operatorname{sech}\left(h\,Ha\,\sqrt{1+\lambda_1}\right)\right)\right) - \left(y\right)\left(\frac{Gr\beta}{Ha^2}\frac{\partial h}{\partial x}\right)hy. \tag{16}$$

By using boundary condition $v|_{y=h} = \frac{\partial h}{\partial t}$ in equation (16), the expression for rate of wall deformation can be evaluated as:

$$\frac{\partial h}{\partial t} = \frac{1}{Ha^2}\frac{\partial^2 p}{\partial x^2}\left(h - \frac{\tanh\left(h\,Ha\,\sqrt{1+\lambda_1}\right)}{Ha\,\sqrt{1+\lambda_1}}\right) + \tanh^2\left(h\left(Ha\left(\sqrt{1+\lambda_1}\right)\right)\right)\frac{\partial h}{\partial x}\left(\frac{1}{Ha^2}\frac{\partial p}{\partial x} + \frac{Gr\beta}{Ha^4(1+\lambda_1)} - \frac{Gr}{Ha^2}\right) - \frac{Gr\beta}{Ha^2}\frac{\partial h}{\partial x}h^2. \tag{17}$$

The axial pressure gradient is calculated by integratig equation (17) with respect to x and can be expressed as:

$$\frac{\partial p}{\partial x} = \frac{Ha^2\left\{\int_0^x \frac{\partial h}{\partial t}dx - \left(h - \frac{\tanh\left(h\left(Ha\left(\sqrt{1+\lambda_1}\right)\right)\right)}{Ha\left(\sqrt{1+\lambda_1}\right)}\right)\left(\frac{Gr\beta}{Ha^4(1+\lambda_1)} - \frac{Gr}{Ha^2}\right) + \frac{Gr\beta}{Ha^2}\frac{h^3}{3} - G_0(t)\right\}}{h - \frac{\tanh\left(h\left(Ha\left(\sqrt{1+\lambda_1}\right)\right)\right)}{Ha\left(\sqrt{1+\lambda_1}\right)}}. \tag{18}$$

In this context, $G_0(t)$ is an arbitrary constant which can further be evaluated as:

$$G_0(t) = \frac{\Delta p_L - \int_0^l \frac{Ha^2\left\{\int_0^x \frac{\partial h}{\partial t}dx - \left(h - \frac{\tanh\left(h\left(Ha\left(\sqrt{1+\lambda_1}\right)\right)\right)}{Ha\left(\sqrt{1+\lambda_1}\right)}\right)\left(\frac{Gr\beta}{Ha^4(1+\lambda_1)} - \frac{Gr}{Ha^2}\right) + \frac{Gr\beta}{Ha^2}\frac{h^3}{3}\right\}}{h - \frac{\tanh\left(h\left(Ha\left(\sqrt{1+\lambda_1}\right)\right)\right)}{Ha\left(\sqrt{1+\lambda_1}\right)}}dx}{\int_0^l \frac{Ha^2}{\frac{\tanh\left(h\left(Ha\left(\sqrt{1+\lambda_1}\right)\right)\right)}{Ha\left(\sqrt{1+\lambda_1}\right)} - h}dx}.\psi \tag{19}$$

The volumetric flow rate Q quantifies the volume of fluid flowing through a designated point in a pipe or channel within a specified time interval and is determined as:

$$Q = \int_0^h udy = \frac{1}{Ha\,\sqrt{1+\lambda_1}}\left(\frac{1}{Ha^2}\frac{\partial p}{\partial x} + \frac{Gr\beta}{Ha^4(1+\lambda_1)} - \frac{Gr}{Ha^2}\tanh\left(h\left(Ha\left(\sqrt{1+\lambda_1}\right)\right)\right) - \frac{1}{Ha^2}\frac{\partial p}{\partial x}h - \frac{Gr\beta}{Ha^2}\frac{h^3}{6} - \frac{Grh}{Ha^2}\frac{\beta}{Ha^2(1+\lambda_1)} - 1\right).\psi \tag{20}$$

Stream function (ψ) can also be computed as:

Downloaded from http://ftp.nowpublishers.com/hff/article-pdf/35/8/2813/10338472/hff-11-2024-0898en.pdf by guest on 01 June 2026

$$\psi = \frac{1}{Ha^2}\frac{\partial p}{\partial x}\left(\frac{\sinh\ y\ Ha\ \sqrt{1+\lambda_1}))}{\cosh\ h\ Ha\sqrt{(1+\lambda_1)}\leftarrow}\left(-y\right) + \frac{1}{Ha\sqrt{(1+\lambda_1)}\leftarrow}\frac{\sinh\ y\ Ha\ \sqrt{1+\lambda_1}))}{\cosh\ h\ Ha\sqrt{(1+\lambda_1)}\leftarrow}\left(\frac{Gr\beta}{Ha^4(1+\lambda_1)\leftarrow} - \frac{Gr}{Ha^2}\right.\right.$$
$$\left.\left. + \frac{Gr\beta}{Ha^2}\frac{h^2}{2}y - \left(\frac{Gr\beta}{Ha^2}\frac{y^3}{6} - \frac{Gry}{Ha^2}\right)\frac{\beta}{Ha^2(1+\lambda_1)\leftarrow} - 1\right) . \quad (21)$$

The wall shear stress is an essential factor in characterizing fluid flow, as it is affected by resistive forces, and is defined and computed as:

$$\tau|_{y=h} = \frac{\partial u}{\partial y}|_{y=h} = Ha\ \sqrt{1+\lambda_1}\left(\frac{1}{Ha^2}\frac{\partial p}{\partial x} + \frac{Gr\beta}{Ha^4(1+\lambda_1)\leftarrow} - \frac{Gr}{Ha^2}\quad tanh\ \ h\ \ Ha\ \ \sqrt{1+\lambda_1}\left(\quad - \frac{Gr\beta h}{Ha^2}\right).\psi \quad (22)$$

The Nusselt number quantifies the heat transfer rate caused by fluid motion in a thermofluidic system, and is mathematically expressed as:

$$Nu = \frac{\partial h}{\partial x}\frac{\partial \theta}{\partial y}|_{y=h}.\psi \quad (23)$$

2.5 Entropy generation

Entropy generation refers to the rise in entropy within a system because of the irreversibilities like heat transfer, friction and mixing, indicating the degree of energy dissipation, which can be defined as:

$$\overline{EG} = \frac{k}{T_0}\quad \left(\frac{\partial T}{\partial \overline{x}}\right)^2 + \left(\frac{\partial T}{\partial \overline{y}}\right)^2\Bigg)\Bigg(+\frac{\mu}{T_0}\quad 2\quad \left(\frac{\partial \overline{u}}{\partial \overline{x}}\right)^2 + \left(\frac{\partial \overline{v}}{\partial \overline{y}}\right)^2\Bigg) + \left(\frac{\partial \overline{u}}{\partial \overline{y}} + \frac{\partial \overline{v}}{\partial \overline{x}}\right)^2\Bigg).\Bigg(\psi \quad (24)$$

Further it can be expressed in the nondimensional form as:

$$EG = \frac{\overline{EG}}{EG_0}.\psi \quad (25)$$

Here, $EG = \frac{k(\Delta T)^2}{T_0{}^2 b^2}$, and $\Delta T = (T_1 - T_0)$ represent the temprature difference between the wall and the center of the channel, and the normalized form of entropy generation can further be expessed as:

$$EG = \left(\frac{\partial \theta}{\partial y}\right)^2 + \frac{Br}{\Lambda T}\left(\frac{\partial u}{\partial y}\right)^2.\psi \quad (26)$$

Here, $Br = \frac{\mu u_0^2}{k\Delta T}$ is Brinkmann number and $\Lambda T = \frac{\Delta T}{T_0}$ is relative temprature.

3. Results and discussion

This study investigates the thermal behavior of Jeffrey fluid flow in the presence of a magnetic field, induced by rhythmic membrane propagation with varying time phase lags. Jeffrey fluid and membrane-based microchannels are chosen for their broad applicability. The governing equations are solved analytically, and MATLAB software is used to generate graphs and evaluate the effects of physical parameters ranges including Hartmann number

Downloaded from http://ftp.nowpublishers.com/hff/article-pdf/35/8/2813/10338472/hff-11-2024-0898en.pdf by guest on 01 June 2026

(*Ha* = 1–3), Grashof number (*Gr* = 1–5), heat source parameter (β = 1–7), Jeffrey fluid parameter (λ_1 = 1–7), membrane shape parameter (*M* = 2–6), relative temperature (ΛT = 0.1–0.9) and Brinkmann number (*Br* = 0.1–0.9) (Kumar *et al.*, 2024; Bhandari *et al.*, 2022b). The results include an analysis of entropy generation, pressure distribution, pressure gradient, heat transfer rate, axial and transverse velocities, volumetric flow rate and wall shear stress. The dimensionless form for the membrane wall is expressed as:

$$h(x,t)=\begin{cases}\frac{1}{2} & -\frac{L}{2}\le x<-a\\ \frac{1}{2}+2a_0\left(\frac{x}{a}^{2M}-1\right)^3 h_{memb}(x,t) & -a\le x\le a\\ \frac{1}{2} & a<x\le\frac{L}{2}\end{cases},\psi \tag{27}$$

The outcomes of this study can be examined as follows.

3.1 Velocity profile

Figures 2(a-d) provides the comparative analysis for the fluid driven by two mechanisms: pressure-driven flow (due to a pressure gradient created at the inlet of the channel) and fluid flow driven by a membrane. In Figures 2(a, b), the axial velocity profile is analyzed for the various values of Hartmann number in the presence and absence of the buoyancy force. The results clearly show that an increase in the Hartmann number, a dimensionless parameter representing the effect of the Lorentz force, leads to a decrease in axial velocity. This phenomenon occurred for membrane-driven and pressure-driven flow (Bhatti *et al.*, 2016). In the membrane-driven flow, we have considered the external pressure at the inlet to be zero, and for the pressure-driven flow, we have neglected the impact of the flexible membrane by substituting the amplitude of the membrane as zero. Furthermore, Figure 2(c, d) also demonstrate the impact of axial velocity without buoyancy forces, and with buoyancy forces. Figure 2(c) depicts that in the case of pressure-driven flow, an increase in the Jeffrey fluid parameter (λ_1) results in a significant increase in axial velocity. In contrast, when the flow is influenced by membrane action, a rise in λ_1 leads to a notable decrease in axial velocity. These observations strongly indicate that the Jeffrey fluid parameter exerts a more substantial effect on flow characteristics in the absence of buoyancy forces. Figure 2(d) demonstrates that in the presence of buoyancy forces ($Gr \neq 0$), increasing the Jeffrey fluid parameter enhances the axial velocity in both pressure-driven and membrane-driven flows. This observation aligns with previous findings (Bhatti *et al.*, 2016; Vajravelu *et al.*, 2011) and emphasizes the significant influence of buoyancy effects on fluid behavior in microchannels.

Figure 3(a) illustrates that the axial velocity increases with a higher Grashof number in both pressure-driven and membrane-driven flows. This behavior aligns with findings in prior studies (Vajravelu *et al.*, 2011), as the Grashof number represents buoyancy effects. Enhanced buoyancy promotes fluid acceleration, thereby elevating axial velocity in both flow mechanisms. Figure 3(b) shows that an increase in heat source parameters enhanced axial velocity, highlighting the strong impact of thermal energy on the flow's dynamics. This indicates that thermal inputs enhance fluid movement along the axis, underscoring the critical role of heat generation in modifying the flow behavior. Figure 4 presents a comparative analysis of axial velocity profiles for the pressure-driven (a_0 = 0) and membrane-driven flows (p_0 = 0). The solid lines represent the pressure-driven flow and the dots (•) denote the membrane-driven flow. The results reveals that both flow types exhibit

Downloaded from http://ftp.nowpublishers.com/hff/article-pdf/35/8/2813/10338472/hff-11-2024-0898en.pdf by guest on 01 June 2026

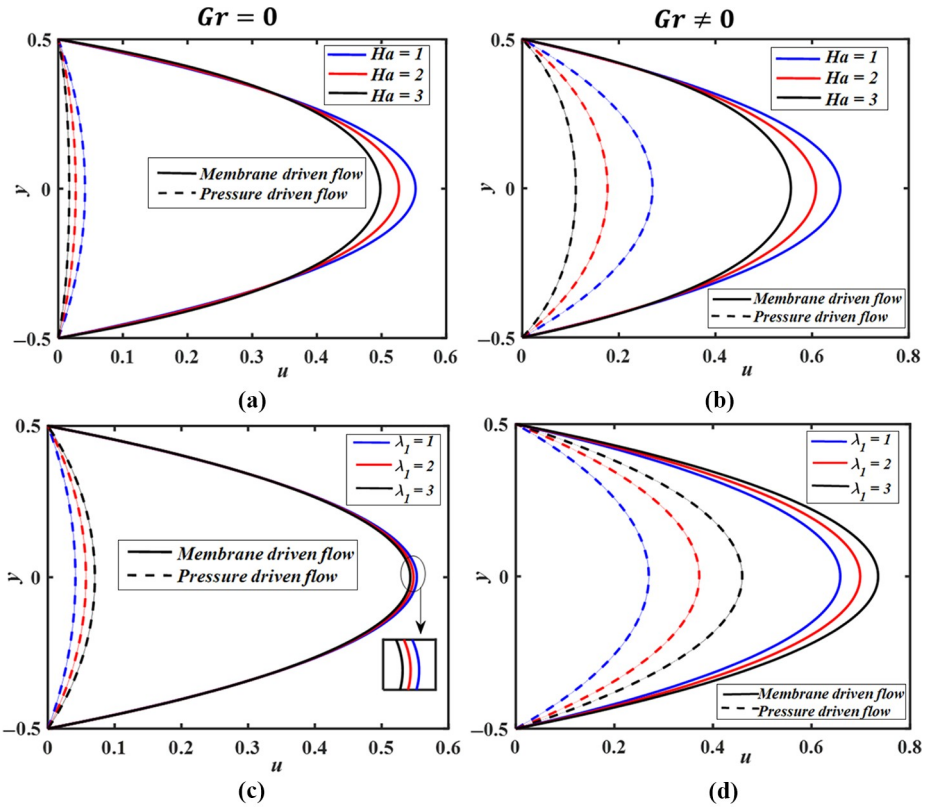

Source(s): Figure by authors

Figure 2. Comparative analysis of axial velocity between pressure-driven flow and membrane driven flow for different values of (a, b) Hartmann number (*Ha*) and (c, d) Jeffrey fluid parameter (λ_1), at fixed values of $\beta = 1$, $t = 0.25$ and $x = 0.75$

similar behavior when inlet pressure is set at p_0 = 1.91, 2.23, 2.71 and the membrane amplitude is a_0 = 0.2, 0.23, 0.27. This finding highlights the comparable influence of these parameters on flow dynamics, providing valuable insights for optimizing fluid systems in various applications.

Figures 5(a-d) analyze the impact of numerous parameters like the Hartmann number (*Ha*), Grashof number (*Gr*), heat source parameter (β) and Jeffrey fluid parameter (λ_1) on transverse velocity. Figure 5(a) illustrates the effect of the Hartmann number (*Ha*) on the transverse velocity profile. At lower *Ha* values, the transverse velocity profile diminished and smoother, reflecting weaker magnetic damping. Figure 5(b) depicts the influence of the Grashof number (*Gr*), revealing that as *Gr* increases, the transverse velocity also increases (Bhandari and Tripathi, 2022). Further, Figures 5(c, d) illustrate that the transverse velocity rises with an increase in both the heat source parameter and the Jeffrey fluid parameter. The heat source parameter amplifies thermal and buoyancy-driven forces (Bhandari and Tripathi, 2022), while the Jeffrey fluid parameter adjusts the fluid's

Downloaded from http://ftp.nowpublishers.com/hff/article-pdf/35/8/2813/10338472/hff-11-2024-0898en.pdf by guest on 01 June 2026

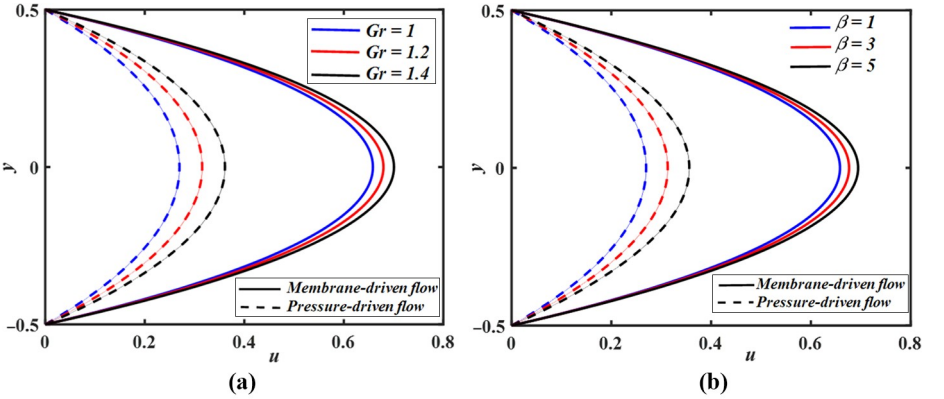

Source(s): Figure by authors

Figure 3. Comparative analysis of axial velocity between pressure-driven flow and membrane driven flow for different values of (a) Grashof number (Gr) and (b) heat source parameter (β), at fixed values of $Ha = 1, \lambda_1 = 1, t = 0.25$ and $x = 0.75$

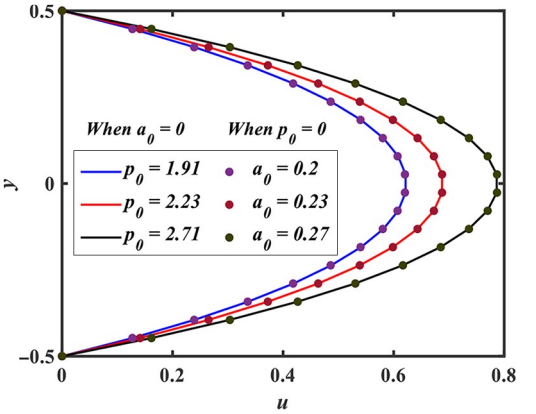

Source(s): Figure by authors

Figure 4. Comparative analysis of axial velocity between pressure-driven flow and membrane driven flow for different values of inlet pressure (p_0), and amplitude of the membrane (a_0), at fixed values of $Ha = 1, \lambda_1 = 1, Gr = 1, \beta = 1, t = 0.25$ and $x = 0.75$

behaviour, enabling more pronounced velocity variations. Physically, the heat source parameter intensifies thermal and buoyancy-driven forces within the fluid, promoting enhanced fluid motion. Meanwhile, the Jeffrey fluid parameter characterizes the fluid's viscoelastic properties, influencing its responsiveness to the driving forces. As this parameter increases, the fluid becomes more adaptable to these thermal and buoyancy effects, resulting in greater transverse velocity variations. This interplay highlights how thermal energy sources and fluid elasticity synergistically affect the flow dynamics, leading to notable velocity augmentation.

Downloaded from http://ftp.nowpublishers.com/hff/article-pdf/35/8/2813/10338472/hff-11-2024-0898en.pdf by guest on 01 June 2026

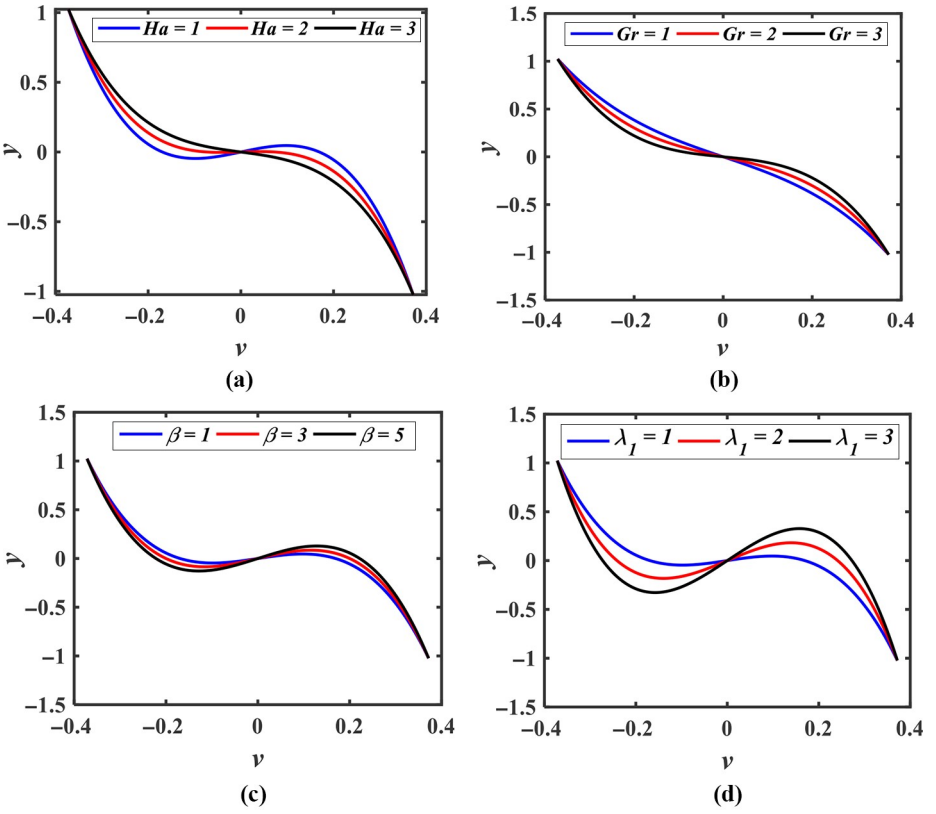

Source(s): Figure by authors

Figure 5. Transverse velocity profiles for different values of (a) Hartmann number (*Ha*), (b) Grashof number (*Gr*), (c) heat source parameter (β) and (d) Jeffrey fluid parameter (λ_1) for fixed values of $M = 2$, $a = 0.2$, $a_0 = 0.2$, $k_0 = 9.95$, $t = 0.25$, $x = 0.5$

3.2 Pressure gradient

Figures 6(a-d) illustrate the changes in the axial pressure gradient for the of Hartmann number (*Ha*), Grashof number (*Gr*), heat source parameter (β) and Jeffrey fluid parameter (λ_1). Figure 6(a) elucidates the variation in axial pressure gradient for different values of Hartmann number (*Ha*). The higher values of *Ha* enhance the magnetic field's damping effect on fluid flow, necessitating a greater pressure gradient to sustain the same flow rate due to the suppression of fluid motion (Bhandari *et al.*, 2020). Figure 6(b) shows that higher the Grashof number implying the stronger buoyancy forces which enhance fluid motion, leading to a reduced pressure gradient required to maintain the same flow rate. Figure 6(c) shows that as the heat source parameter increases, fluid temperature rises, reducing viscosity and lowering the pressure gradient. Additionally, Jeffrey fluid parameter (λ_1) influences the fluid's viscoelastic behavior, which is the ratio of relaxation to retardation time, affecting its overall flow dynamics and response to external forces. As shown in Figure 6(d), enhancing the ratio of relaxation times amplifies the elastic effects, influencing flow behavior and the

Downloaded from http://ftp.nowpublishers.com/hff/article-pdf/35/8/2813/10338472/hff-11-2024-0898en.pdf by guest on 01 June 2026

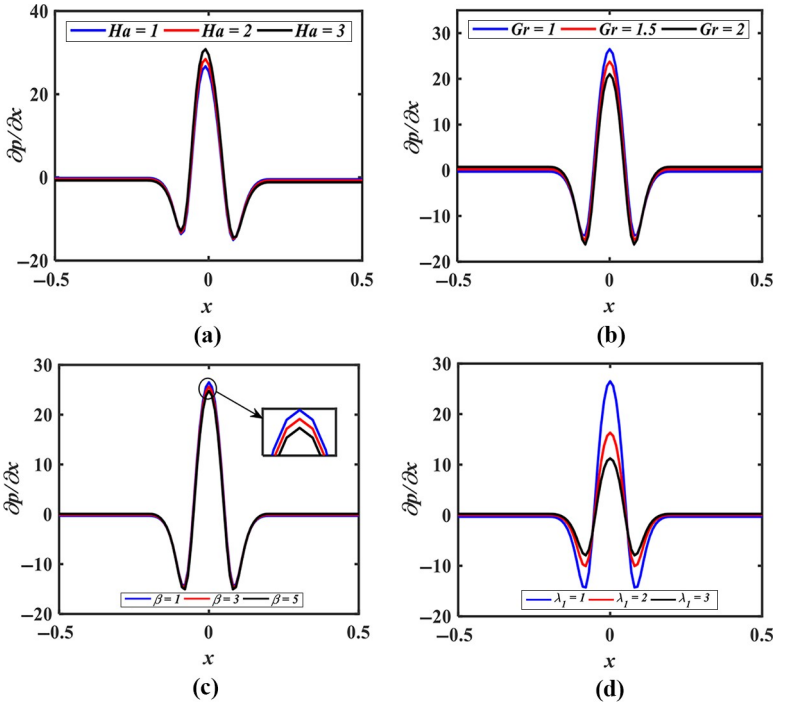

Source(s): Figure by authors

Figure 6. Pressure gradient for different values of (a) Hartmann number (*Ha*), (b) Grashof number (*Gr*), (c) heat source parameter (β) and (d) Jeffrey fluid parameter (λ_1) at the transition phase with the fixed values $M = 2$, $a = 0.2$, $a_0 = 0.2$, $k_0 = 9.95$

pressure gradient see. In membrane-based pumping systems, a higher ratio results in a reduction of the pressure gradient, as the elastic properties of the fluid become more prominent. This change alters the overall flow dynamics, highlighting the significant impact of relaxation time ratios on the pumping performance and pressure distribution in the system.

3.3 Pressure distribution

3.3.1 Compression phase. Pressure distribution is the variation of pressure within a microchannel during fluid flow, which helps to explain the fluid behavior under various conditions. In a symmetrical microchannel utilizing membrane-based pumping, the pressure distribution during the compression phase ($t = 0.25$) is significantly affected by the membrane's motion. The maximum pressure occurs at the microchannel's center, where the membrane is integrated. Figures 7(a-d) illustrate how various parameters influence this pressure distribution. Figure 7(a) highlights the impact of the Hartmann number (*Ha*), showing that an increase in *Ha* leads to enhace pressure distribution. Figure 7(b) examines the effect of the Grashof number (*Gr*) during the compression phase (Bhandari *et al.*, 2020). As *Gr* increases, the pressure distribution rises, reflecting the dominance of buoyant forces over viscous forces, which enhances natural convection and elevates pressure (Bhandari *et al.*, 2022b). Similarly, Figure 7 (c) demonstrates that as the heat source parameter (β) increases, the pressure distribution also

Downloaded from http://ftp.nowpublishers.com/hff/article-pdf/35/8/2813/10338472/hff-11-2024-0898en.pdf by guest on 01 June 2026

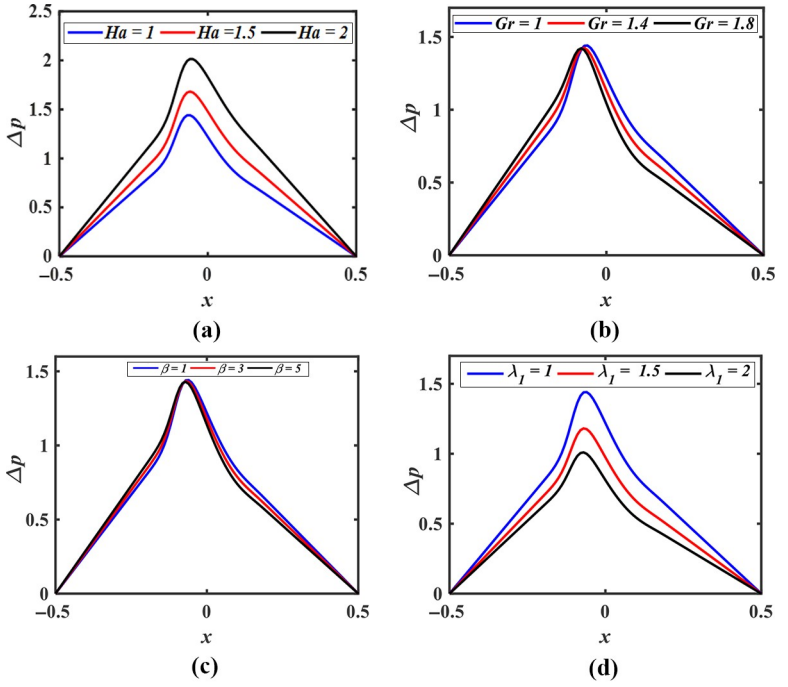

Source(s): Figure by authors

Figure 7. Pressure distribution at compression phase (t = 0.25) for different value of (a) Hartmann number (Ha), (b) Grashof number (Gr), (c) heat source parameter (β) and (d) Jeffrey fluid parameter (λ_1) at expansion phase with the fixed values M = 2, a = 0.2, a_0 = 0.2, k_0 = 9.95

rises. This indicates that a higher β leads to elevated temperature, stronger buoyancy-driven convection, and increased pressure (Bhandari *et al.*, 2022b). Finally, Figure 7(d) explores the effect of the Jeffrey fluid parameter (λ_1), revealing that a higher λ_1 significantly diminishesh the pressure distribution. This underscores the influence of elastic effects, as a larger Jeffrey fluid parameter intensifies pressure during membrane compression.

3.3.2 Expansion phase. During the expansion phase (t = 0.75), the results are similar to those in Figures 8(a-d), but exhibit an inverse effect, as illustrated in Figures 8(a-d). This difference is attributed to the increased cross-sectional area available for fluid flow during expansion phase. The impact of various parameters including the Hartmann number (Ha), Grashof number (Gr), heat source parameter (β) and Jeffrey fluid parameter (λ_1) is evident in this phase. In Figure 8(a), with an increase in Ha, a rise in pressure distribution can be seen, which behaves oppositely compared to the contraction phase (t = 0.25) (Bhandari *et al.*, 2020). This is due to the movement between the magnetic field and fluid flow. For other parameters like Grashof number (Gr), heat source parameter (β) and Jeffrey fluid parameter (λ_1), an increase in their values reduces pressure distribution during the expansion phase (t = 0.75), which again shows a reversed trend compared to the contraction phase (t = 0.25). This reduction suggests that buoyancy forces, heat generation and elastic effects have a less pronounced impact on the fluid during expansion, requiring less pressure to drive the flow.

Downloaded from http://ftp.nowpublishers.com/hff/article-pdf/35/8/2813/10338472/hff-11-2024-0898en.pdf by guest on 01 June 2026

3.4 Volumetric flow rate

The volumetric flow rate is analyzed for a viscoelastic fluid in membrane-based pumping, considering factors such as Hartmann number (*Ha*), Grashof number (*Gr*), heat source parameter (β) and Jeffrey fluid parameter (λ_1) for viscoelastic fluid in membrane-based pumping. In Figure 9(a), as *Ha* increases, the Lorentz force (due to magnetic field) becomes stronger, decreasing the fluid flow leads to a reduction in the volumetric flow rate. Figure 9 (b) shows that a higher Grashof number (*Gr*), which corresponds to stronger buoyancy forces, enhances the volumetric flow rate. The heat source parameter (β) represents internal heat generation within the fluid. An increase in β raises the fluid's temperature, influencing viscosity, density and flow rate. Figure 9(c) demonstrates that an increase in β leads to a higher volumetric flow rate. Bhandari *et al.* (Bhandari *et al.*, 2022b) reported a comparable trend, noting that an increase in the Grashof number was associated with a rise in the volumetric flow rate. Finally, Figure 9(d) illustrates the role of the Jeffrey fluid parameter (λ_1) in defining the viscoelastic properties of the Jeffrey fluid. A higher λ_1 suggests more pronounced viscoelastic effects, which can enhance resistance to deformation, thereby lowering the volumetric flow rate. These parameters collectively influence the dynamics of fluid flow in the system.

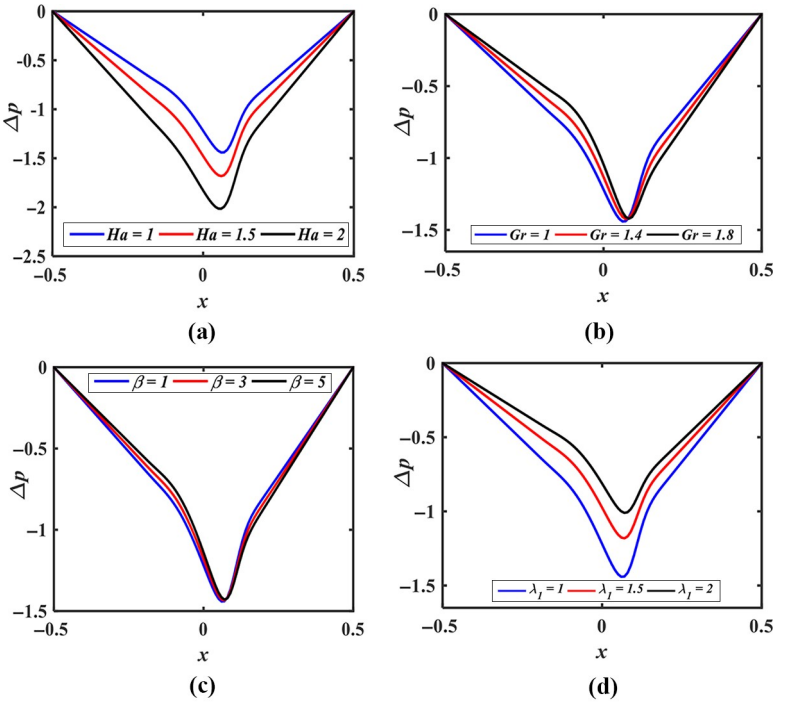

Source(s): Figure by authors

Figure 8. Pressure distribution at expansion phase for different value of (a) Hartmann number (*Ha*), (b) Grashof number (*Gr*), (c) heat source parameter (β) and (d) Jeffrey fluid parameter (λ_1) at expansion phase ($t = 0.75$) with the fixed values $M = 2$, $a = 0.2$, $a_0 = 0.2$, $k_0 = 9.95$

Downloaded from http://ftp.nowpublishers.com/hff/article-pdf/35/8/2813/10338472/hff-11-2024-0898en.pdf by guest on 01 June 2026

3.5 Heat transfer rate (Nusselt number)

The Nusselt number (*Nu*) is a dimensionless quantity that quantifies the ratio of convective to conductive heat transfer at a fluid boundary. It is commonly used to assess heat transfer efficiency, especially in fluid flow applications like heat exchangers. Mathematically, it can be expressed as: $Nu = \frac{\partial h}{\partial x} \frac{\partial \theta}{\partial y} |_{y=h}$. The Nusselt number is analyzed for different membrane shape parameters (M) and heat source parameter (β) to understand their effect on heat transfer. In Figure 10(a), the Nusselt number remains zero throughout the channel except where membranes are attached, indicating that membrane-based pumping enhances heat transfer in those areas. The largest variation occurs when the membrane shape parameter is $M = 6$, where fluctuations are more pronounced due to the high amplitude at $t = 0.5$. Figure 10(b) shows the effect of the heat source parameter (β) on the Nusselt number, with convective heat transfer increasing as β rises (Bhandari and Tripathi, 2022). When $\beta = 6$, more significant fluctuations are observed, similar to those seen with membrane shape parameters, demonstrating that both membrane shapes and heat sources significantly influence heat transfer dynamics within the system.

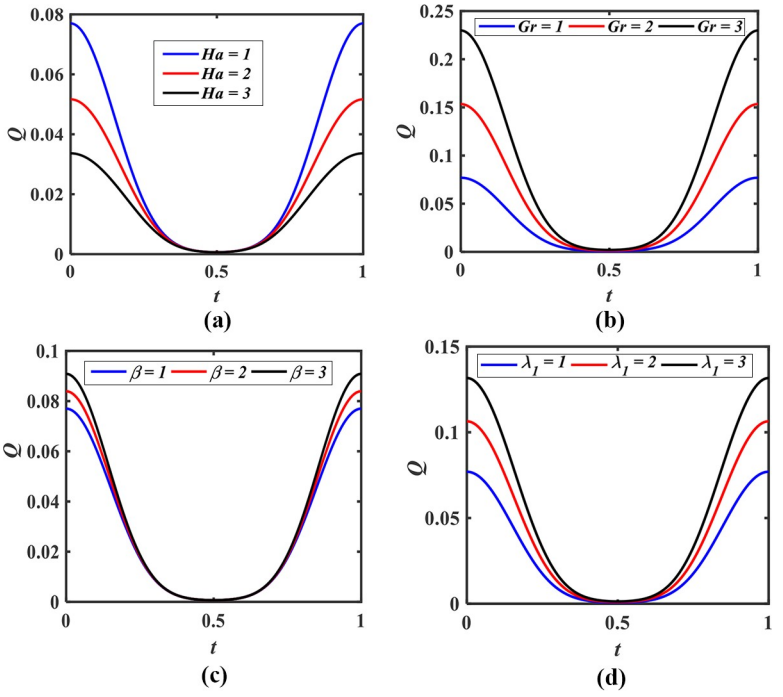

Source(s): Figure by authors

Figure 9. Volumetric flow rate for different values of (a) Hartmann number (*Ha*), (b) Grashof number (*Gr*), (c) heat source parameter (β) and (d) Jeffrey fluid parameter (λ_1) at expansion phase ($t = 0.75$) with the fixed values $M = 2$, $a = 0.2$, $a_0 = 0.2$, $k_0 = 9.95$

Downloaded from http://ftp.nowpublishers.com/hff/article-pdf/35/8/2813/10338472/hff-11-2024-0898en.pdf by guest on 01 June 2026

3.6 Entropy generation

Entropy generation (*EG*) quantifies a system's irreversibility, reflecting the loss of usable energy caused by inefficiencies such as heat transfer and fluid friction. It is mathematically expressed as: $EG = \left(\frac{\partial\theta}{\partial y}\right)^2 + \frac{Br}{\Lambda T}\left(\frac{\partial u}{\partial y}\right)^2$. The first term, $\left(\frac{\partial\theta}{\partial y}\right)^2$, represents thermal dissipation, while the second term, $\left(\frac{\partial u}{\partial y}\right)^2$, accounts for viscous dissipation. The Brinkman number $Br = \frac{\mu u_0^2}{k\Delta T}$ quantifies viscous heating in the fluid, and $\Lambda T = \frac{\Delta T}{T_0}$ represents relative temperature. The variation in entropy generation with parameters such as Hartmann number (*Ha*), Grashof number (*Gr*), heat source parameter (β), Jeffrey fluid parameter (λ_1), membrane shape parameter (*M*), Brinkman number (*Br*) and relative temperature (ΛT) is analyzed through Figures 11(a-d) and 12(a-c). Figure 11(a) shows that increasing the Hartman number (*Ha*), which demonstrates the impact of a magnetic field on fluid flow, typically suppresses fluid motion due to magnetic damping. This reduction in flow decreases viscous dissipation, leading to lower entropy generation associated with viscous effects. In contrast, Figure 11(b) demonstrates that a higher Grashof number (*Gr*) results in stronger buoyancy forces, which increase fluid motion. Figures 11(c, d) further reveal that both the heat source parameter (β) and Jeffrey fluid parameter (λ_1) increases the entropy generation. The presence of a heat source parameter raises the fluid's temperature, enhancing thermal dissipation (Bhandari and Tripathi, 2022), while a higher λ_1 value, representing the fluid's viscoelasticity, adds to the complexity of the flow and increases viscous dissipation, thus contributing to higher entropy. Moving to Figures 12(a-c), Figure 12(a) indicates that increasing the membrane shape parameter (*M*) enhances fluid flow, leading to increased entropy generation (Bhandari and Tripathi, 2022). As the membrane deforms, the fluid motion becomes more intense, driving higher dissipation rates. Figures 12(b, c) examine the impact of the Brinkman number (*Br*) and relative temperature (ΛT) on entropy generation profile. A higher Brinkman number leads to an increased entropy generation, signifying greater energy loss due to frictional heating. However, an increase in relative temperature (ΛT) shows the opposite effect, reducing entropy generation (Bhandari and Tripathi, 2022). This inverse relationship suggests that higher temperatures lower the

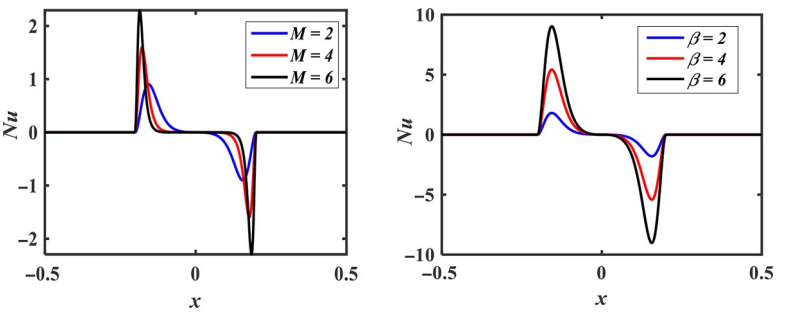

Source(s): Figure by authors

Figure 10. Variation in heat transfer rate (Nusselt number) for different value of (a) membrane shape parameter (m) and (b) heat source parameter (β) at the fixed values $a = 0.2$, $a_0 = 0.2$, $k_0 = 9.95$, $t = 0.5$

Downloaded from http://ftp.nowpublishers.com/hff/article-pdf/35/8/2813/10338472/hff-11-2024-0898en.pdf by guest on 01 June 2026

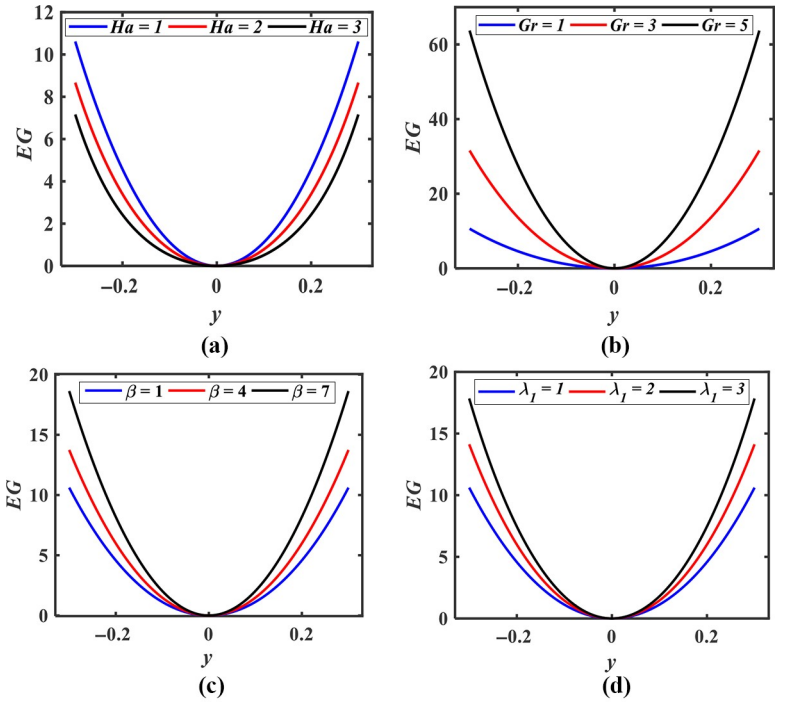

Source(s): Figure by authors

Figure 11. Entropy generation for different values of (a) Hartmann number (*Ha*), (b) Grashof number (*Gr*), (c) heat source parameter (β) and (d) Jeffrey fluid parameter (λ_1) with the fixed values $M = 2$, $a = 0.2$, $a_0 = 0.2$, $k_0 = 9.95$, $Br = 0.5$, $\Lambda T = 0.5$, $t = 0.25$, $x = 0.5$

temperature gradients within the fluid, reducing thermal dissipation and overall entropy production.

3.7 Wall shear stress

Figures 13(a-d) show the variation in wall shear stress (τ) along the wall for different parameter values, including Hartmann number (*Ha*), Grashof number (*Gr*), heat source parameter (β) and the Jeffrey fluid parameter (λ_1). In Figure 13(a), it is observed that the wall shear stress peaks in the contraction region due to membrane movement. The effect of varying *Ha* on wall shear stress is examined, revealing that an increase in *Ha*, which indicates the magnetic field's influence on fluid flow, results in higher wall shear stress (Bhandari *et al.*, 2020). This is attributed to the stronger Lorentz force at higher *Ha*, which increases flow resistance. Figure 13(b) shows that higher Grashof number, representing stronger buoyancy force, reduce local wall shear stress, which implies fluid flow is enhanced (Bhandari and Tripathi, 2022). Figure 13(c) indicates that increasing the heat source parameter decreases wall shear stress, likely due to the thermal effects reducing viscosity and weakening fluid resistance (Bhandari and Tripathi, 2022). Finally, Figure 13(d) demonstrates that as the Jeffrey fluid parameter (λ_1) increases, the viscoelastic nature of the Jeffrey fluid leads to a reduction in wall shear stress, as the fluid becomes more resistant to deformation.

Downloaded from http://ftp.nowpublishers.com/hff/article-pdf/35/8/2813/10338472/hff-11-2024-0898en.pdf by guest on 01 June 2026

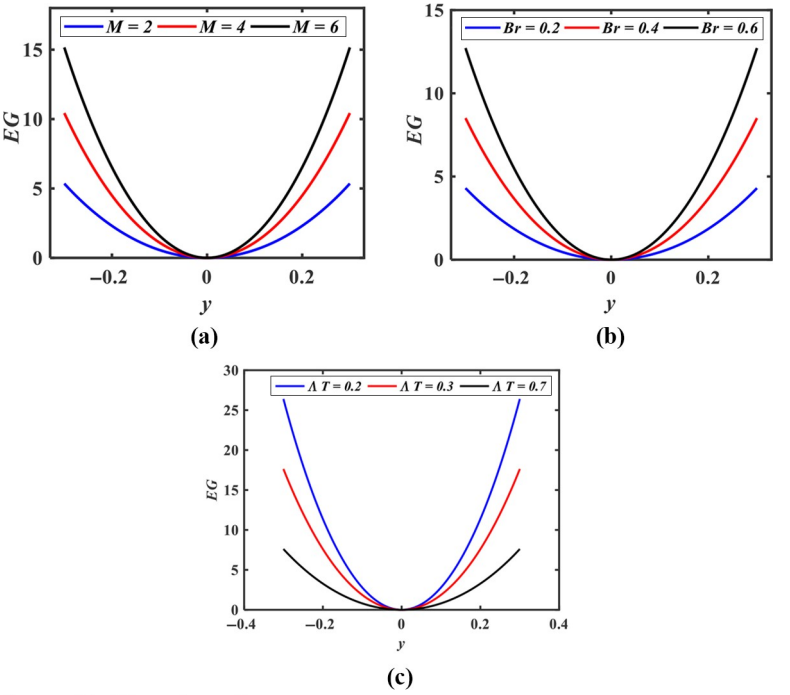

Source(s): Figure by authors

Figure 12. Entropy generation for different values of (a) membrane shape parameter (m), (b) Brinkman number (Br) and (c) relative temperature (ΛT) at the time $t = 0.25$ and position $x = 0.5$ for the fixed values $a = 0.2$, $a_0 = 0.2$, $k_0 = 9.95$, $Ha = 1$, $\beta = 1$, $Gr = 1$, $\lambda_1 = 1$

3.8 Streamlines

Contour plots for the stream function during the transition phase ($t = 0.5$) for varying values of the Hartmann number (Ha), Grashof number (Gr), heat source parameter (β), Jeffrey fluid parameter (λ_1), membrane shape parameter (M) and time variation (t) are depicted in Figures 14(a-f). Figure 14(a) shows how the Hartmann number affects the streamlines. As Ha increases, the magnitude of the stream function decreases, indicating that higher Hartmann number suppresses fluid flow due to the magnetic damping effect. Figure 14(b) highlights the effect of the Grashof number, where an increase in Gr leads to a rise in the stream function magnitude, reflecting enhanced fluid flow. Figures 14(c, d) illustrate the impact of the heat source parameter (β) and Jeffrey fluid parameter (λ_1) on the streamlines. In Figure 14(c), a higher heat source parameter increases the stream function, suggesting that internal heating enhances fluid motion. In Figure 14(d), the Jeffrey fluid parameter, which define the characteristics of viscoelastic fluids i.e., Jeffrey fluids, is shown to amplify the stream function. Higher λ_1 values make the fluid more elastic, allowing it to store and release energy efficiently, promoting more vigorous fluid flow in the presence of heat transfer. In Figure 14(e), the membrane shape parameter (M) is examined. As the membrane shape parameter increases, so does the stream function, altering the membrane shape can modify fluid motion, offering a potential means of controlling flow patterns. Figure 14(f) shows stream patterns at different time phases. During the contraction phase, the stream function

Downloaded from http://ftp.nowpublishers.com/hff/article-pdf/35/8/2813/10338472/hff-11-2024-0898en.pdf by guest on 01 June 2026

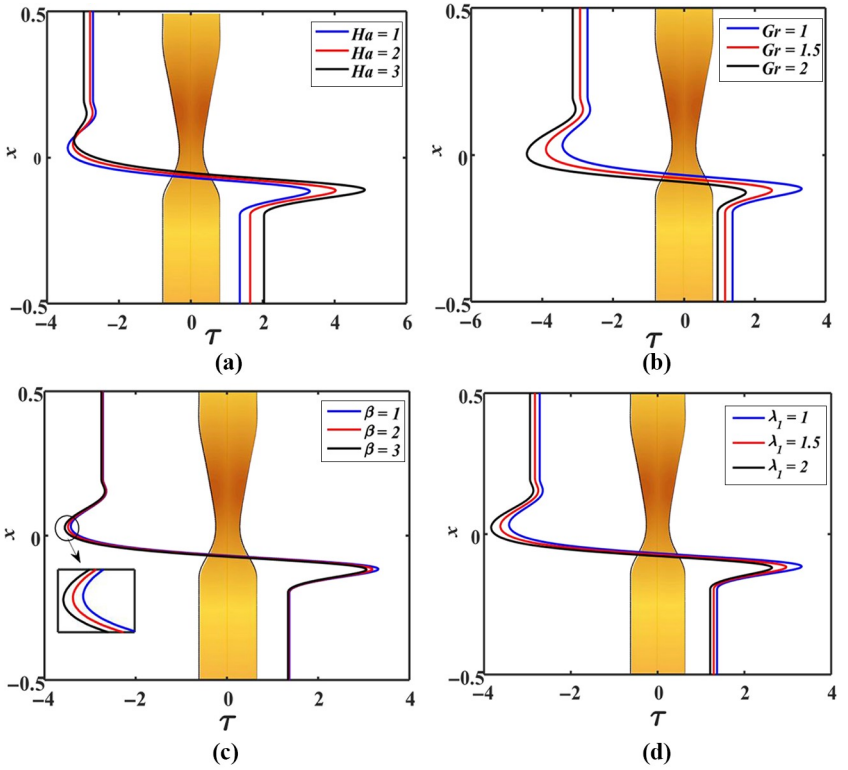

Source(s): Figure by authors

Figure 13. Wall shear stress at compression phase (t = 0.25) for different values of (a) Hartmann number (Ha), (b) Grashof number (Gr), (c) heat source parameter (β) and (d) Jeffrey fluid parameter (λ_1) at the fixed values M = 2, a = 0.2, a_0 = 0.2, k_0 = 9.95

magnitude is higher, indicating that the fluid is being compressed and accelerated. In contrast, during the transition phase, the stream function is lower, signaling a shift in flow dynamics. In the expansion phase, the stream function decreases as the cross-sectional area through which the fluid flows increases, suggesting a reduction in flow rate. This reverse behavior in the stream function indicates that as the microchannel expands, the fluid slows down, reflecting the fluid's transition through different flow states.

3.9 Isotherms

Figure 15(a, b) presents contour plots of isotherms for varying heat source parameters (β) and time phases (t). Figure 15(a) examines the effect of heat source parameter at the contraction phase (t = 0.25). The results show that as the heat source parameter rises, the contour plots exhibit a noticeable increase in the magnitude of the contour plots of isotherms. This indicates that higher heat source values lead to a more intense thermal response in the flow. Figure 15(b) explores the impact of different time phases including the contraction, transition and expansion phases, on the contour plots. It is also observed that the temperature reaches

Downloaded from http://ftp.nowpublishers.com/hff/article-pdf/35/8/2813/10338472/hff-11-2024-0898en.pdf by guest on 01 June 2026

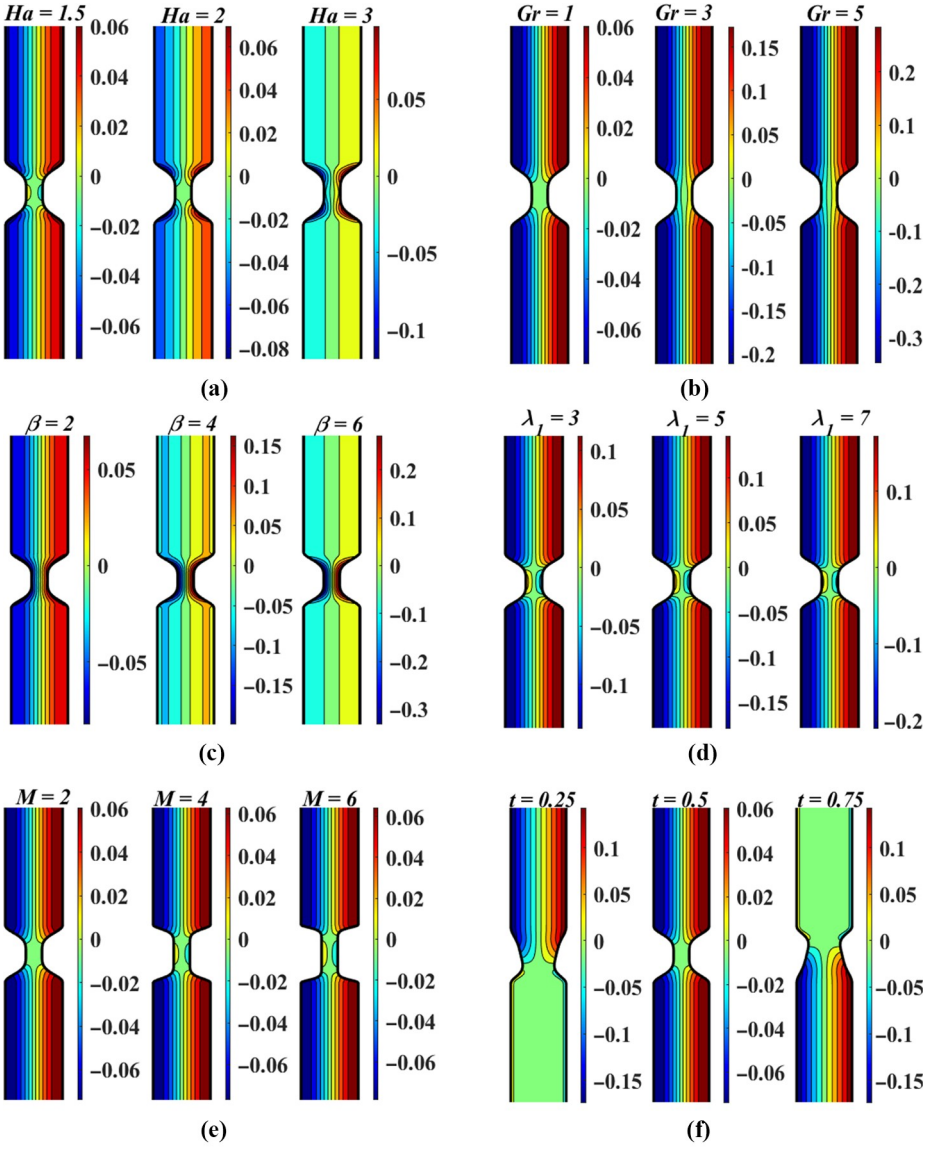

Source(s): Figure by authors

Figure 14. Streamlines at transition phase ($t = 0.5$) for different values of (a) Hartmann number (Ha) when $M = 2$, $Gr = \lambda_1 = \beta = 1$, (b) Grashof number ($Gr$) when $Ha = \lambda_1 = \beta = 1$, $M = 2$, (c) heat source parameter (β) when $M = 2$, $Gr = Ha = \lambda_1 = 1$, (d) Jeffrey fluid parameter (λ_1) when $M = 2$, $Ha = Gr = \beta = 1$, (e) shape of the membrane (M) when $Ha = Gr = \beta = 1$ and (f) different time phase when $M = 2$, $Ha = Gr = \beta = 1$

Downloaded from http://ftp.nowpublishers.com/hff/article-pdf/35/8/2813/10338472/hff-11-2024-0898en.pdf by guest on 01 June 2026

maximum at the center of the microchannel, suggesting that higher heat source parameters intensify the temperature gradient.

3.10 Velocity distribution

Figures 16(a, b) illustrate the contour plots for the axial velocity and transverse velocity at the different times $t = 0.25$, $t = 0.5$ and $t = 0.75$. In Figure 16(a), the axial velocity profile illustrates the fluid speed distribution along the channel length. It is noted that during the transition phase ($t = 0.5$), the axial velocity is lower compared to the compression and expansion phases, due to maximum compression of the microchannel. Additionally, Figure 16(b) shows that the transverse velocity is minimal during the transition phase when compared to the compression and expansion phases. The transverse velocity also varies where the membrane is fitted within the microchannel.

4. Conclusions

This study investigated the membrane-driven flow and heat transfer of viscoelastic fluids under magnetic field influence. This study demonstrates the significant impact of transverse magnetic field, membrane deformation on viscoelastic fluid flow and heat transfer. A comparative analysis between membrane driven flow and pressure driven flow in absence and presence of buyancy force has also been presented. Moreover, entropy generation has been discussed. The key findings include:

- The axial velocity decreases as the Hartmann number increases, but it increases with higher values of the Grashof number, heat source parameter and Jeffrey fluid parameter.
- The pressure increases with an increase in the Hartmann number, but decreases as the Grashof number, heat transfer rate and Jeffrey fluid parameter rise.
- The heat transfer rate (Nusselt number) increases with higher values of the membrane shape parameter and heat source parameter.
- The wall shear stress increases with the Hartmann number but decreases as the Grashof number, heat transfer rate and Jeffrey fluid parameter increase.

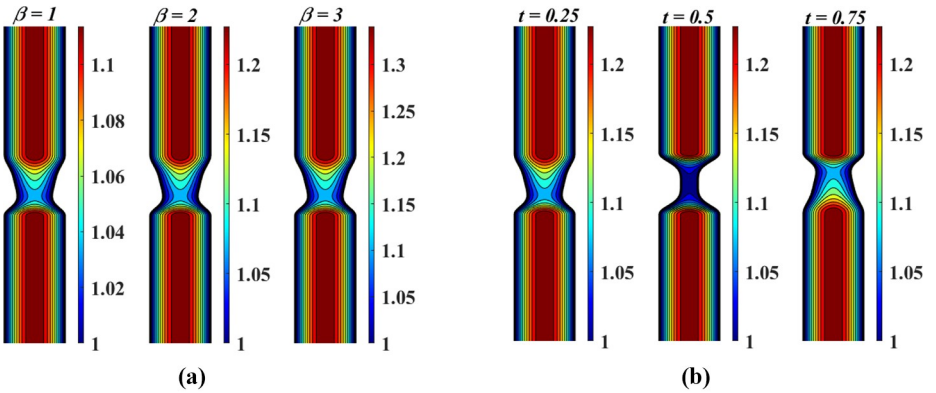

Source(s): Figure by authors

Figure 15. Isotherms (θ) for different values of (a) heat source parameter (β) and (b) for different time phase (t) when $Gr = Ha = \lambda_1 = 1$, $M = 2$

Downloaded from http://ftp.nowpublishers.com/hff/article-pdf/35/8/2813/10338472/hff-11-2024-0898en.pdf by guest on 01 June 2026

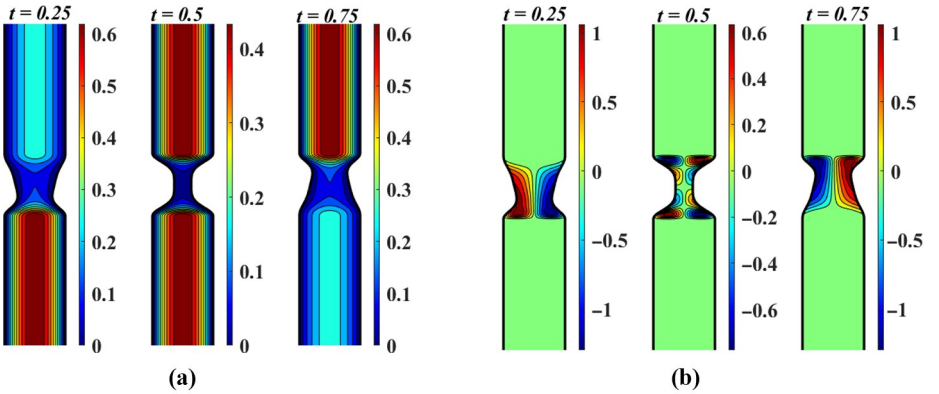

Source(s): Figure by authors

Figure 16. Contour plots for (a) axial velocity and (b) transverse velocity for compression phase (t = 0.25), transition phase (t = 0.5) and expansion phase (t = 0.75) at fixed values of $Ha = \lambda_1 = 1$, $M = Gr = 2$

- Entropy generation decreases with an increase in the Hartmann number and relative temperature, but increases with higher values of the Grashof number, heat transfer rate, Jeffrey fluid parameter, Brinkman number and membrane shape parameter. Increasing the Hartman number reduces the magnitude of the stream function, indicating that stronger magnetic fields suppress fluid flow due to magnetic damping, while higher Grashof numbers and heat source parameters enhance the flow.
- As the heat source parameter rises, the isotherms intensify, showing a more significant thermal response in the flow, with maximum temperatures concentrated at the center of the microchannel during the contraction phase.

The findings provide valuable insights for optimizing membrane-based systems, enhancing heat transfer efficiency and advancing applications in biomedical and industrial fields. This study establishes a foundation for future research on the thermal behavior of non-Newtonian fluids under magnetic fields. Future investigations can build upon this work by exploring complex geometries, varying magnetic field configurations and different non-Newtonian fluids. The ultimate goal is to optimize membrane-driven systems for industrial applications in biomedical engineering, aerospace and renewable energy, improving efficiency and sustainability.

References

Aboelkassem, Y. and Staples, A.E. (2013), "A bioinspired pumping model for flow in a microtube with rhythmic wall contractions", *Journal of Fluids and Structures*, Vol. 42, pp. 187-204.

Akbar, N.S., Nadeem, S. and Ali, M. (2011), "Jeffrey fluid model for blood flow through a tapered artery with a stenosis", *Journal of Mechanics in Medicine and Biology*, Vol. 11 No. 3, pp. 529-545.

Aslam, M.N., Riaz, A., Shaukat, N., Aslam, M.W. and Alhamzi, G. (2024), "Machine learning analysis of heat transfer and electroosmotic effects on multiphase wavy flow: a numerical approach", *International Journal of Numerical Methods for Heat and Fluid Flow*, Vol. 34 No. 1, pp. 150-177.

Downloaded from http://ftp.nowpublishers.com/hff/article-pdf/35/8/2813/10338472/hff-11-2024-0898en.pdf by guest on 01 June 2026

Bhandari, D.S. and Tripathi, D. (2022), "Study of entropy generation and heat flow through a microtube induced by the membrane-based thermofluidics systems", *Thermal Science and Engineering Progress*, Vol. 34, p. 101395.

Bhandari, D.S., Tripathi, D. and Anwar Bég, O. (2022a), "Electro-osmosis modulated periodic membrane pumping flow and particle motion with magnetic field effects", *Physics of Fluids*, Vol. 34 No. 9.

Bhandari, D.S., Tripathi, D. and Prakash, J. (2022b), "Insight into Newtonian fluid flow and heat transfer in vertical microchannel subject to rhythmic membrane contraction due to pressure gradient and buoyancy forces", *International Journal of Heat and Mass Transfer*, Vol. 184, p. 122249.

Bhandari, D.S., Tripathi, D. and Narla, V.K. (2020), "Magnetohydrodynamics-based pumping flow model with propagative rhythmic membrane contraction", *The European Physical Journal Plus*, Vol. 135 No. 11, p. 890.

Bhatti, M.M., Ellahi, R. and Zeeshan, A. (2016), "Study of variable magnetic field on the peristaltic flow of Jeffrey fluid in a non-uniform rectangular duct having compliant walls", *Journal of Molecular Liquids*, Vol. 222, pp. 101-108.

Bhatti, M., Munawwar, A.A. and Muhammad, S. (2024), "Optimizing fluid flow efficiency: third-grade hybrid nanofluid flow with electro-magneto-hydrodynamics in confined vertical spaces", *Nanofluids*, Elsevier, Amsterdam, pp. 243-275.

Bhatti, M.M., Sait, S.M., Ellahi, R., Sheremet, M.A. and Oztop, H. (2022), "Thermal analysis and entropy generation of magnetic Eyring-Powell nanofluid with viscous dissipation in a wavy asymmetric channel", *International Journal of Numerical Methods for Heat and Fluid Flow*, Vol. 33 No. 5, pp. 1609-1636.

Böhme, G. and Friedrich, R. (1983), "Peristaltic flow of viscoelastic liquids", *Journal of Fluid Mechanics*, Vol. 128 No. 1, pp. 109-122.

Cai, Z., Xiang, J., Chen, H. and Wang, W. (2016), "Membrane-based valves and inward-pumping system for centrifugal microfluidic platforms", *Sensors and Actuators B: Chemical*, Vol. 228, pp. 251-258.

Elelamy, A.F., Elgazery, N.S. and Ellahi, R. (2020), "Blood flow of MHD non-Newtonian nanofluid with heat transfer and slip effects: application of bacterial growth in heart valve", *International Journal of Numerical Methods for Heat and Fluid Flow*, Vol. 30 No. 11, pp. 4883-4908.

Ellahi, R. (2013), "The effects of MHD and temperature dependent viscosity on the flow of non-Newtonian nanofluid in a pipe: analytical solutions", *Applied Mathematical Modelling*, Vol. 37 No. 3, pp. 1451-1467.

Ellahi, R. and Hameed, M. (2012), "Numerical analysis of steady non-Newtonian flows with heat transfer analysis, MHD and nonlinear slip effects", *International Journal of Numerical Methods for Heat and Fluid Flow*, Vol. 22 No. 1, pp. 24-38.

Ellahi, R., Rahman, S.U. and Nadeem, S. (2014), "Blood flow of Jeffrey fluid in a catherized tapered artery with the suspension of nanoparticles", *Physics Letters A*, Vol. 378 No. 40, pp. 2973-2980.

Esmael, A., Nouar, C., Lefevre, A. and Kabouya, N. (2010), "Transitional flow of a non-Newtonian fluid in a pipe: experimental evidence of weak turbulence induced by shear-thinning behavior", *Physics of Fluids*, Vol. 22 No. 10.

Farooq, M., Gull, N., Alsaedi, A. and Hayat, T. (2015), "MHD flow of a Jeffrey fluid with Newtonian heating", *Journal of Mechanics*, Vol. 31 No. 3, pp. 319-329.

Hayat, T., Ali, N. and Asghar, S. (2007), "An analysis of peristaltic transport for flow of a Jeffrey fluid", *Acta Mechanica*, Vol. 193 Nos 1/2, pp. 101-112.

Hayat, T., Asad, S., Mustafa, M. and Alsaedi, A. (2015), "MHD stagnation-point flow of Jeffrey fluid over a convectively heated stretching sheet", *Computers and Fluids*, Vol. 108, pp. 179-185.

Downloaded from http://ftp.nowpublishers.com/hff/article-pdf/35/8/2813/10338472/hff-11-2024-0898en.pdf by guest on 01 June 2026

Hosseini, S.M., Manzari, M.T. and Hannani, S.K. (2007), "A fully explicit three-step SPH algorithm for simulation of non-Newtonian fluid flow", *International Journal of Numerical Methods for Heat and Fluid Flow*, Vol. 17 No. 7, pp. 715-735.

Idowu, A.S., Joseph, K.M. and Daniel, S. (2013), "Effect of heat and mass transfer on unsteady MHD oscillatory flow of Jeffrey fluid in a horizontal channel with chemical reaction", *IOSR Journal of Mathematics*, Vol. 8 No. 5, pp. 74-87.

Kothandapani, M. and Pushparaj, V. (2017), "Consequence of induced magnetic field on peristaltic motion of a Carreau nanofluid in a tapered asymmetric channel", *International Journal of Numerical Methods for Heat and Fluid Flow*, Vol. 27 No. 9, pp. 1986-2014.

Kumar, A., Bhardwaj, A. and Tripathi, D. (2024), "Peristaltic pumping of viscoelastic fluid in a diverging channel: effects of magnetic field and surface roughness", *International Journal of Numerical Methods for Heat and Fluid Flow.*

Liao, S.-J. (2003), "On the analytic solution of magnetohydrodynamic flows of non-Newtonian fluids over a stretching sheet", *Journal of Fluid Mechanics*, Vol. 488, pp. 189-212.

Lindner, A., Bonn, D., Poiré, E.C., Amar, M.B. and Meunier, J. (2002), "Viscous fingering in non-Newtonian fluids", *Journal of Fluid Mechanics*, Vol. 469, pp. 237-256.

Magesh, A. and Kothandapani, M. (2021), "Heat and mass transfer analysis on non-Newtonian fluid motion driven by peristaltic pumping in an asymmetric curved channel", *The European Physical Journal Special Topics*, Vol. 230 No. 5, pp. 1447-1464.

Metzner, A.B. (1965), "Heat transfer in non-Newtonian fluids", *Advances in Heat Transfer*, Elsevier, Amsterdam, Vol. 2, pp. 357-397.

Nadeem, S. and Akbar, N.S. (2009), "Peristaltic flow of a Jeffrey fluid with variable viscosity in an asymmetric channel", *Zeitschrift Für Naturforschung A*, Vol. 64 No. 11, pp. 713-722.

Pandey, S.K. and Tripathi, D. (2010), "Unsteady model of transportation of Jeffrey-fluid by peristalsis", *International Journal of Biomathematics*, Vol. 3 No. 4, pp. 473-491.

Pandey, A., Kumar, A., Tripathi, D. and Sharma, K. (2024), "Transient flow of electrolyte solution in porous media with membranes fitted at the upper wall surface and lower charged surface", *Microfluidics and Nanofluidics*, Vol. 28 No. 10, p. 69.

Prommas, R. (2011), "Theoretical and experimental study of heat and mass transfer mechanism during convective drying of multi-layered porous packed bed", *International Communications in Heat and Mass Transfer*, Vol. 38 No. 7, pp. 900-905.

Ramadan, S.F., Mekheimer, K.S., Bhatti, M.M. and Khalique, C.M. (2025), "Induced magnetic field and thermal regulation of synovial fluid flow through irregular surfaces with first-order slip and gold nanoparticles", *Separation Science and Technology*, Vol. 60 No. 1, pp. 133-156.

Sen, S.S.S., Das, M. and Shaw, S. (2021), "Thermal dispersed homogeneous-heterogeneous reaction within MHD flow of a Jeffrey fluid in the presence of Newtonian cooling and nonlinear thermal radiation", *Heat Transfer*, Vol. 50 No. 6, pp. 5744-5759.

Shaw, S., Moitoi, A.J. and Shit, G.C. (2023), "Fractionalized Jeffrey fluid model for predicting magnetic nanoparticles trajectory: a physiological aspects of drug targeting", *Chinese Journal of Physics*, Vol. 83, pp. 214-230.

Shojaeian, M. and Koşar, A. (2014), "Convective heat transfer and entropy generation analysis on Newtonian and non-Newtonian fluid flows between parallel-plates under slip boundary conditions", *International Journal of Heat and Mass Transfer*, Vol. 70, pp. 664-673.

Tripathi, D. (2011), "Peristaltic transport of a viscoelastic fluid in a channel", *Acta Astronautica*, Vol. 68 Nos 7/8, pp. 1379-1385.

Tripathi, D. and Bég, O.A. (2012), "Magnetohydrodynamic peristaltic flow of a couple stress fluid through coaxial channels containing a porous medium", *Journal of Mechanics in Medicine and Biology*, Vol. 12 No. 5, p. 1250088.

Downloaded from http://ftp.nowpublishers.com/hff/article-pdf/35/8/2813/10338472/hff-11-2024-0898en.pdf by guest on 01 June 2026

Tripathi, D., Bhandari, D.S. and Bég, O.A. (2023), "A critical review on micro-scale pumping based on insect-inspired membrane kinematics", *Sensors and Actuators A: Physical*, Vol. 360, p. 114518.

Tsai, R., Huang, K.H. and Huang, J.S. (2008), "Flow and heat transfer over an unsteady stretching surface with non-uniform heat source", *International Communications in Heat and Mass Transfer*, Vol. 35 No. 10, pp. 1340-1343.

Turkyilmazoglu, M. and Pop, I. (2013), "Exact analytical solutions for the flow and heat transfer near the stagnation point on a stretching/shrinking sheet in a Jeffrey fluid", *International Journal of Heat and Mass Transfer*, Vol. 57 No. 1, pp. 82-88.

Vajravelu, K., Sreenadh, S. and Lakshminarayana, P. (2011), "The influence of heat transfer on peristaltic transport of a Jeffrey fluid in a vertical porous stratum", *Communications in Nonlinear Science and Numerical Simulation*, Vol. 16 No. 8, pp. 3107-3125.

Yadeta, H.B. and Shaw, S. (2023), "Analysis of unsteady non-Newtonian Jeffrey blood flow and transport of magnetic nanoparticles through an inclined porous artery with stenosis using the time fractional derivative", *Journal of Applied Physics*, Vol. 134 No. 10.

Yoshino, M., Hotta, Y-h., Hirozane, T. and Endo, M. (2007), "A numerical method for incompressible non-Newtonian fluid flows based on the lattice Boltzmann method", *Journal of Non-Newtonian Fluid Mechanics*, Vol. 147 Nos 1/2, pp. 69-78.

Yusuf, A., Bhatti, M.M. and Khalique, C.M. (2024), "Computational study of the thermophysical properties of graphene oxide/vacuum residue nanofluids for enhanced oil recovery", *Journal of Thermal Analysis and Calorimetry*, Vol. 150 No. 1, pp. 1-13.

About the authors

Abhishesh Pandey is working as a Research Scholar in Manipal University Jaipur, Jaipur since 2023. He obtained his Master's degree in Mathematics from the University of Allahabad in 2021. His research focuses on the mathematical modeling and analysis of rheological phenomena in physiological systems.

Ashvani Kumar is working as a Research scholar in the National Institute of Technology, Uttarakhand, since 2022. He completed the Master degree in Mathematics from Gurukul Kangri Vishwavidyalaya, Haridwar, in 2020. His research topic is in rheological studies of fluid flow in physiological systems.

Dharmendra Tripathi has been working as Associate Professor in Department of Mathematics, National Institute of Technology, Uttarakhand. He has completed his PhD in Applied Mathematics (Mathematical Modeling of Physiological flows) in 2009 from Indian Institute of Technology BHU and MSc in Mathematics from Banaras Hindu University.

His research work is focused on the mathematical modeling and simulation of biological flows in deformable domains, peristaltic flow of Newtonian and non-Newtonian fluids, membrane-based pumping flow models; dynamics of various infectious diseases; microfluidics; CFD, biomechanics; heat transfer; nanofluids; energy systems; numerical methods; etc.

He has supervised eight PhD students and five are working under his supervision. He has also guided 20 B. Tech projects. He has published more than 240 papers in reputed international journals, 3 edited Book in Springer, 2 edited Book in CRC, 10 book chapters and presented more than 40 papers in International and National Conferences. His research h-index is 59 and i-10 index is 192 and his papers have more than 9,975 citations as per Google Scholar data base. He has been listed in top 2% researchers/scientist across the World as per Updated science-wide author databases of standardized citation indicators in year 2020 and year 2021. He has received Best Faculty Award for year 2022 by NIT Uttarakhand, Best Researcher Award by ITSR in 2023, President Award in 2017 by the Manipal University Jaipur for outstanding contribution, Prof PR Sharma Memorial award from International Academy for Physical Sciences (IAPS) in 2021 and also become Associate Fellow of IAPS in 2022.

Kalpna Sharma is currently Professor and Head at the Department of Mathematics and Statistics and joined Manipal University Jaipur. She has an extensive teaching and administrative experience of over 25 years. She had successfully handled several diverse responsibilities such as Associate Dean (I

Downloaded from http://ftp.nowpublishers.com/hff/article-pdf/35/8/2813/10338472/hff-11-2024-0898en.pdf by guest on 01 June 2026

Year), Head of the Department, NSS Coordinator, Faculty in charge of Rotaract Club, center superintendent for RTU, Academic Coordinator, Convener of Library Advisory Committee at different institutions. Sharma coordinated Ph.D. program of Manipal University Jaipur from 2015 to 2020. She is presently presiding officer of the Internal Committee of the University also. On her credit, she has published number of papers in peer reviewed journals, awarded two patents, three copyrights and presented papers in National/International conferences. She has delivered lectures as invited talk, keynote speaker and chaired number of sessions at International/National Conferences. Currently she is guiding seven research scholars and five scholars completed their PhD under her guidance. Kalpna Sharma is the corresponding author can be contacted at: kalpana.sharma@jaipur.manipal.edu

For instructions on how to order reprints of this article, please visit our website:
www.emeraldgrouppublishing.com/licensing/reprints.htm
Or contact us for further details: **permissions@emeraldinsight.com**

Downloaded from http://ftp.nowpublishers.com/hff/article-pdf/35/8/2813/10338472/hff-11-2024-0898en.pdf by guest on 01 June 2026